Integrated PDR/GNSS at Different Times for Pedestrian Localization in Urban Canyon

XIANGHONG LI[ID][1,2], **DONGYAN WEI**[2], **WENCHAO ZHANG**[ID][2], **YING XU**[ID][2], **AND HONG YUAN**[ID][2]

[1]School of Electronic, Electrical and Communication Engineering, University of Chinese Academy of Sciences, Beijing 100049, China

[2]Aerospace Information Research Institute, Chinese Academy of Sciences, Beijing 100094, China

Corresponding author: Xianghong Li (lixianghong@aircas.ac.cn)

ABSTRACT Smartphone-based pedestrian localization is still a challenge in deep urban canyons, where GNSS signals suffer from the degrading of signal transmission, multipath effects, and NLOS reception. This paper presents a comprehensive pedestrian localization scheme based on PDR and GNSS observations at different times, using the internal sensors equipped in the smartphone, including GNSS raw measurements (pseudo-range, carrier phase), internal MEMS sensor (including the gyroscope, accelerometer, magnetometer, and barometer). The core algorithm utilizes historical effective satellite observation and PDR to solve pedestrian position, exploiting both PDR and GNSS's complementary properties. The proposed approach can improve accuracy and continuity and solve the problem of missing data, such as without satellite coverage. Besides, we design a Kalman filter model to reduce systematic errors and correct PDR in real-time to decrease the cumulative error of PDR. To evaluate the proposed pedestrian localization scheme's performance, we perform experiments in a typical urban canyon with dense foliage and tall buildings and compare it with the different state-of-the-art approaches. The comparison and analysis of the overall positioning performance show that the method proposed in this paper can provide a better localization scheme, and the RMS value of positioning error is improved from 51.7m (GNSS only) to 9.6m.

INDEX TERMS PDR, GNSS of different times, calculating position, integrated PDR/GNSS.

I. INTRODUCTION

As Micro-Electro-Mechanical System (MEMS) has been rapidly developed, various kinds of smart-devices for consumers, such as smartphones, smart-watches, tablet computers, are equipped with Global Navigation Satellite System (GNSS) receivers, and inertial measurement unit (IMU), which provide new and cheap approaches to urban localization.

Commonly the first choice for localization is the GNSS in urban because of its widest coverage. However, pedestrians walk in various kinds of city environments, including open filed, sub-urban streets and deep urban streets. Due to the degrading of signal transmission, notorious multipath effects, and non-line-of-sight (NLOS) reception [1], GNSS cannot achieve highly accurate positioning performance in all areas, especially in urban canyon. Many researchers have proposed combining other positioning methods, such as Pedestrian Dead Reckoning (PDR) [2], visual localization, 3D Maps [3]

The associate editor coordinating the review of this manuscript and approving it for publication was Halil Ersin Soken[ID].

and external signal-aided [4], with GNSS to improve pedestrian navigation capability and stability. According to the unique characteristics of human walking gait, PDR can achieve the user's position by using accelerometers to detect the pedestrian's traveling steps, estimate step length, and use gyro-meters and magnetic estimate heading between every two consecutive steps. And the PDR has the advantage of high precision within short periods, minor calculation and without external equipment. As a result of inaccurate heading direction estimation, inaccurate step length estimation and so on, PDR is easily affected by accumulative errors. So, combining PDR and GNSS will be a highly complementary system.

While the integration of PDR and GNSS is feasible, so many related studies have been published recently. There are a lot of fusion methods for PDR/GNSS. Such as reference [5] develop a prototype system, named GloCal, which combined PDR and GPS to improve the average error concerning GPS. In the study in Reference [6]-[8], traditional filter, like Extended Kalman Filter (EKF) and Unscented Kalman Filter (UKF), was used to estimating the system's

attitude error and the bias of the gyroscope, and it could avoid the accumulation of PDR heading errors over time effectively. Because of the deterioration of received signal quality, some researchers also propose improved filter system, like wavelet transform-based Unscented Kalman Filter (WT-UKF) [9], UKF algorithm used for constraining residual [10]. Besides that, Reference [11] proposed an event-triggered multi-rate size-varying Kalman filter model, which can remove systematic errors due to the wrong calibration of the sensors or environmental noises and solve the integrated problem when sampling rates of each source is different. Those studies have a premise that GNSS can output positioning results because an integrated positioning system mathematical model is established with GNSS and PDR positioning results. But in many areas, like narrow building canyon and dense foliage of street trees, the GNSS receiver cannot provide positioning results. Some researchers use the GNSS carrier phase to solve single-point positioning and integrate GNSS and PDR [12]. But they do the static and kinematic experiment on the playground with an open area without a narrow building canyon and dense foliage of street trees.

Many scholars have proposed fusion methods to deal with the problem of degrading of signal transmission and notorious multipath effects in deep urban canyons, many scholars have proposed fusion methods. Reference [3] proposed a framework of the integration based on 3D map aided GNSS and PDR in the urban canyon with dense foliage. It outputs the stride length and heading of PDR and the position and accuracy of 3D-GNSS into the Kalman filter to obtain the fusion result. Reference [13] presents a comprehensive urban canyon pedestrian navigation scheme. They combine PDR, GNSS and Beacon to calibrate heading and design-related algorithms to adjust or limit the use of these different type observations to constrain large jumps in the Kalman filter model, thereby making the solution stable. Some researchers use GNSS pseudo-range double difference (PDD) and PDR to obtain comprehensive navigation [14], which needs an external base station to provide reference pseudo-range. Those researchers integrate PDR, GNSS and external equipment or assistant, which increase fusion system complexity and cost.

In this paper, we propose a comprehensive approach for fusing GNSS observations and PDR, which only uses the smartphone's internal sensors without external assistance. The proposed fusion method's core algorithm utilizes smartphone internal GNSS raw measurements (pseudo-range, carrier phase) at different times, internal MEMS sensor (including gyroscope, accelerometer, magnetometer, and barometer) to construct a comprehensive positioning solution. The presented solution can solve the localization in a harsh street environment, where the GNSS receiver's position error is substantial and even out of the output. In addition, it can improve pedestrian positioning capability and stability in an urban canyon area. The contributions of this study are as follows.

- We propose a pedestrian localization algorithm based on PDR and GNSS observations at different times, using the smartphone's internal sensors. The core algorithm utilizes historical effective satellite observation and PDR to solve pedestrian position, which exploits the complementary properties of both PDR and GNSS. It can improve accuracy and continuity and solve missing data, such as without satellite coverage.
- We design an equation update method for different situations. As the algorithm presented in this paper utilizes historical observation to solve position, which is different from the traditional ones, we cannot use the general method to update equations. Different updating methods are designed for different measurement data scenarios.
- We design a Kalman filter model to reduce systematic errors and correct PDR in real-time to decrease the cumulative error of PDR. As the PDR is easily affected by accumulative errors and the GNSS has large jumps, a Kalman filter model is designed to smooth these errors.
- We perform experiments in a typical urban canyon with luxuriant trees, high-density tall buildings, and narrow streets to evaluate the proposed pedestrian localization scheme's performance. And we compare it with the different state-of-the-art approaches. Comparing and analyzing the overall positioning performance shows that the method proposed in this paper can provide a better localization scheme.

The rest of this paper is organized as follows: Section 2 introduces the presented algorithm, including calculating position (CalPos) with GNSS observations and PDR at different times, updating equations, integrated PDR/GNSS. Section 3 shows the experimental setup, results and discussion. And finally, Section 5 concludes the paper.

II. METHODOLOGY
When the pedestrian is in a harsh environment, such as dense forests, densely built urban areas, outdoor building corridors, etc., the position error is vast. Sometimes the GNSS receiver cannot output positioning results due to signal blockage and multipath. However, some observations of the GNSS receiver are valid. If we combined the information received at different times, it could meet the requirements of satellite positioning. And the position change of different times can be obtained by PDR, which has high precision in a short period. Therefore, we propose a fusion algorithm to calculate the position based on satellite observation measurement and PDR at different times. As shown in Fig.1, the GNSS receiver receives the north-south satellites' measure at point P1. And when it moves to point P2, the receiver gets the measurement from the east-west satellite. Using data received at P1 and P2 could obtain good Position Dilution of Precision (PDOP), making the positioning accuracy higher.

The fusion algorithm consists of four parts: PDR, CalPos, updating equations, PDR/GNSS, as shown in Fig 2. The internal MEMS sensor measurement (including the gyroscope,
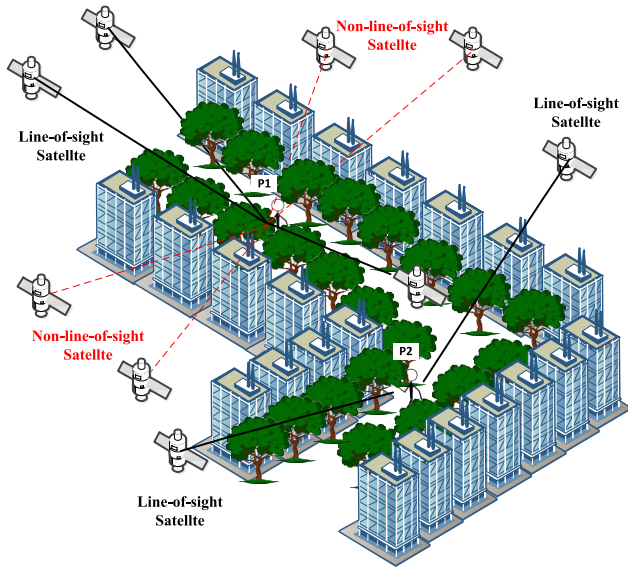
FIGURE 1. Illustration of the foliage attenuation to Line-of-sight Satellite (LOS) and Non-line-of-sight Satellite (NLOS) signals.
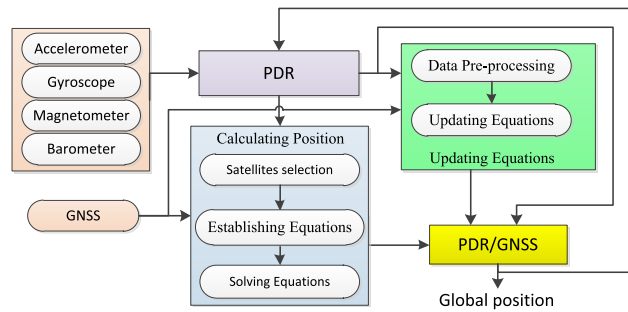

FIGURE 2. Schematic diagram of fusion algorithm.

accelerometer, magnetometer, and barometer) is inputted to the PDR system and output the change of position. The smartphone internal GNSS raw measurements and the output of PDR are inputted into the CalPos part to obtain the localization. The results of PDR and GNSS raw measurements are used to update equations. All the raw data and output are used to calculate PDR/GNSS. They will be introduced as follows.

A. PEDESTRIAN DEAD RECKONING

PDR is an algorithm to estimate pedestrians' movement, which uses the MEMS sensors (accelerometer, gyroscope, and magnetometer) in the smartphone. Pedestrian plane localization can be computed by the previous, moved distance, and pedestrian heading.

$$\begin{cases} x_k^{pdr} = x_{k-1}^{pdr} + SL_k * \sin(heading_k) \\ y_k^{pdr} = y_{k-1}^{pdr} + SL_k * \cos(heading_k) \end{cases} \quad (1)$$

where x_k^{pdr} is the north coordinate of the current location, y_k^{pdr} is the east coordinate of the current location, $heading_k$ is the pedestrian walking orientation and SL_k is the moved distance from the previous step to the current location. To estimate the user's location, there are four steps: step event detection, step length estimation, heading direction estimation and position estimation. We use existing algorithms to solve them [5], [15].

PDR can compute pedestrian plane location. The change in altitude can be calculated with the barometer equipped with the smart device. The relationship between air pressure and elevation is [16]–[18]:

$$dP = -\frac{mPg}{R^*T}dH \quad (2)$$

where P is atmospheric pressure, H is altitude, T is the absolute temperature, m is the molecular weight, g is gravity, and R^* is gas constant. The change of ground temperature is small in a certain period. The influence of the temperature is smaller than that of the pressure. So, the equation can be simplified as

$$\Delta h_k = 18400 * \left(1 + \frac{tp_k}{273.15}\right) * \lg \frac{P_0}{P_k} \quad (3)$$

where tp_k is centigrade, P_0 is the previous pressure. Then the vertical location is

$$h_k^{pdr} = h_{k-1}^{pdr} + \Delta h_k \quad (4)$$

B. CALCULATING POSITION
1) SATELLITE SELECTING
Even though the GNSS's error is substantial or the position cannot be solved, some observation is still useful. So it is necessary to select effective satellites. At present, there are some general satellite selection algorithms, such as the best geometric error factor, the largest tetrahedral volume and the largest determinant [19]. The basic idea is to select the satellite combination with the smallest geometric precision factor. However, the prerequisite for these methods is that the number of satellites is enough and the signal's quality is good. In this paper, we should select the satellite with effectively and relatively good signals when the number of satellites is limited and the signal interference is serious. This article intends to select satellites through the following aspects.

a: BASIC SELECTION
The multipath effect is one of the most important factors that affect the pseudo-range error. Especially when the satellite altitude angle is small, the receiver is easy to receive the multi-path signal reflected by buildings, which makes the pseudo-range error increase. In addition, when the carrier to noise density ratio is small, it means the pseudo-range is influenced by multipath greatly [20]. We can select satellites from the following two aspects: altitude angle $\theta_{i,sj}$ and carrier-to-noise ratio $SNR_{i,sj}$:

$$\begin{cases} flag_b = 1, & if \ (\theta_{i,sj} > Thre_\theta \& SNR_{i,sj} > Thre_{SNR}) \\ flag_b = 0, & otherwise \end{cases} \quad (5)$$

where $Thre_\theta$ and $Thre_{SNR}$ are the threshold of altitude angle and carrier-to-noise ratio. In this paper, the threshold are $Thre_\theta = 7^o$ and $Thre_{SNR} = 35$ for smartphone. When it is satisfied $flag_b = 1$, the satellite can be inputted into next selection part.

The result of satellite selection is shown in Fig.3. Without selecting, the number of satellites is bigger than eight at most times. After basic selection, the number has been reduced by
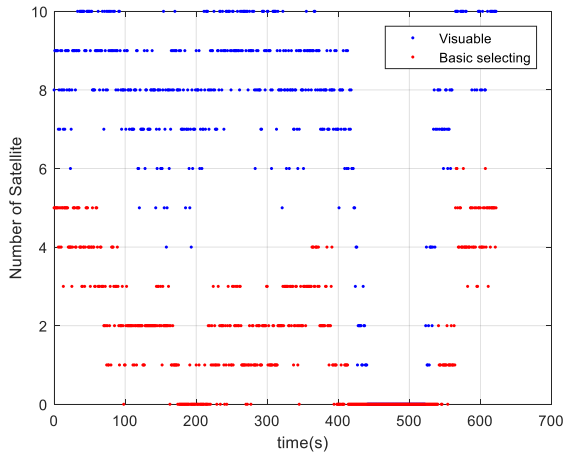
at least four. The total number of satellites is less than four at some time.

b: OBSERVATION SELECTION

The pseudo-range between the satellite to user is [21]

$$\rho_{i,sj} = r_{i,sj} + t_{ui} + t_{i,sj} + I + E + T + \varepsilon_{i,sj} \quad (6)$$

where $r_{i,sj}$ is the real distance between satellite j and user at time i-th, t_{ui} is the clock error of GNSS receiver, $t_{i,sj}$ is the clock error of satellite j, I is the error caused by the ionosphere, E is the ephemeris error, T is the error caused by troposphere, $\varepsilon_{i,sj}$ is the measurement noise including relativistic effect, tidal correction, multipath error, white noise, etc. Some of them can be revised with error models like t_{sj}, I,T and E. After correction, the pseudo-range becomes:

$$\tilde{\rho}_{i,sj} = r_{i,sj} + t_{ui} + \varepsilon_{i,sj} \quad (7)$$

And the difference between two consecutive epochs:

$$\tilde{\rho}_{i+1,sj} - \tilde{\rho}_{i,sj} = (r_{i+,sj} - r_{i,sj}) + (t_{ui+1} - t_{ui}) + (\varepsilon_{i+1,sj} - \varepsilon_{i,sj}) \quad (8)$$

Since the user is a pedestrian, the moving distance within a continuous epoch is very limited, so $r_{i+,sj} - r_{i,sj} \approx 0$.And the receiver clock error within consecutive epochs is unchanged, so $t_{ui+1} - t_{ui} \approx 0$. The formula becomes:

$$d\rho_{i+1,sj} = \tilde{\rho}_{i+1,sj} - \tilde{\rho}_{i,sj} \approx (\varepsilon_{i+1,sj} - \varepsilon_{i,sj}) \quad (9)$$

As $\varepsilon_{i,sj}$ is the measurement noise including relativistic effect, tidal correction, multipath error, white noise and so on, it will not change much within consecutive epochs. In this paper, the difference between two consecutive epochs is used to select the valid observation data as:

$$\begin{cases} flag_{sat} = 1, & if \ |d\rho_{i+1,sj}| < Thre_{sat} \\ flag_{sat} = 0, & otherwise \end{cases} \quad (10)$$

where $Thre_{sat}$ is the threshold. When $flag_{sat} = 1$, the pseudo-range at this time is available.

The result of satellite selection is shown in Fig.4, and the available satellites are shown as red points. The number of satellites is smaller than four at most times. The position
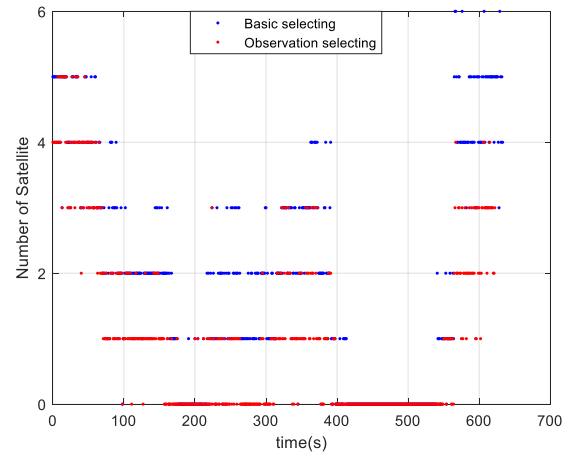
cannot be achieved within a single time. However, if we combined the information at different times, it can meet satellite localization requirements.

2) ESTABLISHING EQUATION

To establish equations for solving position, we suppose that there are n_1 satellites available at time 1-th. The pseud-orange $\rho_{1,j}$ and the position of satellite $(x_{1,sj}, y_{1,sj}, z_{1,sj})$, $j = 1, \ldots, n_1$ are known quantities. The position of the pedestrian (x_1, y_1, z_1) is unknown. The equations between user and satellites can be established as:

$$\begin{cases} \sqrt{(x_{1,s1} - x_1)^2 + (y_{1,s1} - y_1)^2 + (z_{1,s1} - z_1)^2} \\ \quad + t_{u1} = \rho_{1,s1} \\ \qquad \vdots \\ \sqrt{(x_{1,sn1} - x_1)^2 + (y_{1,sn1} - y_i)^2 + (z_{1,sn1} - z_1)^2} \\ \quad + t_{u1} = \rho_{1,sn1} \end{cases} \quad (11)$$

where t_{u1} is the clock error of the GNSS receiver at time 1-th. There are 4 unknowns in those equations. If $n_1 \geq 4$, so those unknowns can be solved. But when $n_1 < 4$, we need more information to solve those equations. The equations are established at time 2-th as:

$$\begin{cases} \sqrt{(x_{2,s1} - x_2)^2 + (y_{2,s1} - y_j)^2 + (z_{2,s1} - z_2)^2} \\ \quad + t_{u2} = \rho_{2,s1} \\ \qquad \vdots \\ \sqrt{(x_{2,sn2} - x_2)^2 + (y_{2,sn2} - y_2)^2 + (z_{2,sn2} - z_2)^2} \\ \quad + t_{u2} = \rho_{2,sn2} \end{cases} \quad (12)$$

And the position relationship between time 1-th and time 2-th is as:

$$\begin{cases} x_1 = x_2 - dx_{1,2} \\ y_1 = y_2 - dy_{1,2} \\ z_1 = z_2 - dz_{1,2} \end{cases} \quad (13)$$

Four unknowns (x_2, y_2, z_2, t_{u2}) and n_2+3 equations are added in the equations. There are eight unknowns and $n_1 + n_2 + 3$ equations in total. If $n_1 + n_2 + 3 \geq 8$, those equations can

be solved. It means that if $n_1 + n_2 < 5$, we need more information. So if we use k epochs to establish equations, we will have $n_1 + n_2 + \cdots + n_k + 3(k-1)$ equations and $4 + 4(k-1)$ unknowns. These equations can be solved as long as it satisfies:

$$n_1 + n_2 + \cdots + n_k + 3(k-1) \geq 4 + 4(k-1),$$
$$(n_i < 4, i = 1 \cdots k, n_i \in N^*) \quad (14)$$

Simplify the inequality:

$$n_1 + n_2 + \cdots + n_k \geq k + 3, \ (n_i < 4, i = 1 \cdots k, n_i \in N^*) \quad (15)$$

Here all parameters satisfy $n_i < 4$, because if any of them is greater than 4 the equations can be solved. The all equations are:

$$
\begin{cases}
\sqrt{(x_{1,s1} - x_1)^2 + (y_{1,s1} - y_1)^2 + (z_{1,s1} - z_1)^2} \\
\quad + t_{u1} = \rho_{1,s1} \\
\vdots \\
\sqrt{(x_{1,sn1} - x_1)^2 + (y_{1,sn1} - y_1)^2 + (z_{1,sn1} - z_1)^2} \\
\quad + t_{u1} = \rho_{1,sn1} \\
\cdots \\
\sqrt{(x_{k,s1} - x_k)^2 + (y_{k,s1} - y_k)^2 + (z_{k,s1} - z_k)^2} \\
\quad + t_{uk} = \rho_{k,s1} \\
\vdots \\
\sqrt{(x_{k,snk} - x_k)^2 + (y_{k,snk} - y_k)^2 + (z_{k,snk} - z_k)^2} \\
\quad + t_{uk} = \rho_{k,snk}
\end{cases} \quad (16)
$$

$$
\begin{cases}
x_1 = x_k - dx_{k,1}, y_1 = y_k - dy_{k,1}, z_1 = z_k - dz_{k,1} \\
x_2 = x_k - dx_{k,2}, y_2 = y_k - dy_{k,2}, z_2 = z_k - dz_{k,2} \\
\vdots \\
x_{k-1} = x_k - dx_{k,k-1}, y_{k-1} = y_k - dy_{k,k-1}, z_{k-1} \\
\quad = z_k - dz_{k,k-1} \\
x_k = x_k, y_k = y_k, z_k = z_k
\end{cases} \quad (17)
$$

where $dx_{k,k-1}$ is the position change of the x-axis from the (k-1)-th to the k-th. And the present (x_k, y_k, z_k) can be solved from those equations.

From the above mathematical analysis, whether the available satellites at different times are the same does not affect the subsequent calculations. However, in practice, if the satellites used for calculation are the same, the equivalent PDOP will be large caused by the poor geometrical distribution of the satellite positions, so that the error of positioning result will be enormous. Therefore, in the actual solution process, in order to ensure the final solution accuracy, it is necessary to determine that four different satellites appear. And this kind of situation exists in reality, as shown in Fig.1.

In addition, the first moment in the above equations can be understood as the first moment in the fixed window length and is not limited to the first moment when the device is started. So the redundant measurement information needs to be eliminated in the case of more observation measurements. In section B will introduce the update equations method.

3) SOLVING EQUATIONS

According to the previous analysis, when the number of available satellites is greater than k + 3, the equations (16) and (17) can be solved. For formula (16), set $\rho_{k,snk}$ as

$$\rho_{k,snk} = f(x, y, z, t_{uk}) \quad (18)$$

Through Taylor expansion of formula (18) at (x_0, y_0, z_0, t_{uk0}) and ignoring the error terms of twice or more, we transform the formula into:

$$
\rho_{k,snk}
$$
$$
= f(x_0, y_0, z_0, t_{uk0}) + \frac{\partial f}{\partial x}\Big|_{(x_0,y_0,z_0,t_{uk0})} (x - x_0)
$$
$$
+ \frac{\partial f}{\partial y}\Big|_{(x_0,y_0,z_0,t_{uk0})} (y - y_0) + \frac{\partial f}{\partial z}\Big|_{(x_0,y_0,z_0,t_{uk0})} (z - z_0)
$$
$$
+ \frac{\partial f}{\partial t_u}\Big|_{(x_0,y_0,z_0,t_{uk0})} (t_{uk} - t_{uk0}) \quad (19)
$$

Which means (20), as shown at the bottom of the page.
So formula (16) and formula (17) is changed to:

$$
\begin{bmatrix} x \\ y \\ z \\ t_{u1} \\ \cdots \\ t_{uk} \end{bmatrix} = \begin{bmatrix} x_0 \\ y_0 \\ z_0 \\ t_{u10} \\ \cdots \\ t_{uk0} \end{bmatrix} + (J^T J)^{-1} J^T \begin{bmatrix} \rho_{1,s1} - (r_{1,s1} - t_{u10}) \\ \vdots \\ \rho_{1,sn1} - (r_{1,sn1} - t_{u10}) \\ \cdots \\ \rho_{k,s1} - (r_{k,s1} - t_{uk0}) \\ \vdots \\ \rho_{k,snk} - (r_{k,snk} - t_{uk0}) \end{bmatrix} \quad (21)
$$

And $J = [J_1 \ J_2]$, where J_1 is Jacobian matrix (22), as shown at the bottom of the next page.

$$
\rho_{k,snk} = (r_{k,snk} + t_{uk0}) + \frac{-(x_{k,snk} - x_0 - dx_{k-1})}{r_{k,snk}} (x - x_0)
$$
$$
+ \frac{-(y_{k,snk} - y_0 - dy_{k-1})}{r_{k,snk}} (y - y_0)
$$
$$
+ \frac{-(z_{k,snk} - z_0 - dz_{k-1})}{r_{k,snk}} (z - z_0) + (t_{uk} - t_{uk0})
$$
$$
r_{k,snk} = \sqrt{(x_{k,snk} - x_0 - dx_{k-1})^2 + (y_{k,snk} - y_0 - dy_{k-1})^2 + (z_{k,snk} - z_0 - dz_{k-1})^2} \quad (20)
$$

And J_2 is

$$J_2 = \begin{bmatrix} J_{21} \\ \vdots \\ J_{2k} \end{bmatrix}_{n \times k}, J_{2i} = \begin{bmatrix} 0 \cdots 0 \ 1 \ 0 \cdots 0 \\ \vdots \ \cdots \ \vdots \ \vdots \ \vdots \ \cdots \ 0 \\ 0 \cdots 0 \ 1 \ 0 \cdots 0 \end{bmatrix}_{ni \times k} \ \textit{ith}$$
(23)

The position of the pedestrian at time k-th can be solved with the formula (21) and Least Square Estimate (LSE) method.

C. UPDATING EQUATIONS

1) DATA PRE-PROCESSING

Since the data frequency of GNSS is lower than the PDR, it's necessary to time-align before calculation. Assume that the previous output time of PDR is k-th, and the GPS output time is j-th that is satisfied with $t_k < t_j < t_{k+1}$. Then estimate the position of PDR at time j as follows:

$$\begin{cases} x_j^{pdr} = x_k^{pdr} + SL_k * \sin(h_k^f) * \dfrac{t_j - t_k}{t_k - t_{k-1}} \\ y_j^{pdr} = y_k^{pdr} + SL_k * \cos(h_k^f) * \dfrac{t_j - t_k}{t_k - t_{k-1}} \\ h_j^{pdr} = h_k^{pdr} + \Delta h_k * \dfrac{t_j - t_k}{t_k - t_{k-1}} \end{cases}$$
(24)

The outputted from PDR is in navigation coordinate system (NCS) and $(dx_{i,j}, dy_{i,j}, dz_{i,j})$ is in the global coordinate system (GCS). So it needs to be converted to GCS:

$$[dx_{i,j}, dy_{i,j}, dz_{i,j}]^T = C_n^g [dx_{i,j}^{pdr}, dy_{i,j}^{pdr}, dh_{i,j}^{pdr}]^T \quad (25)$$

where $\left(dx_{i,j}^{pdr}, dy_{i,j}^{pdr}, dh_{i,j}^{pdr}\right)$ is calculated as:

$$\begin{cases} dx_{i,j}^{pdr} = x_i^{pdr} - x_j^{pdr} \\ dy_{i,j}^{pdr} = y_i^{pdr} - y_j^{pdr} \\ dh_{i,j}^{pdr} = h_i^{pdr} - h_j^{pdr} \end{cases}$$
(26)

And C_n^g is rotation matrix transforming a vector from NCS to GCS, which is calculated as follows [22]:

$$C_n^g = \begin{bmatrix} -\sin L & \cos L & 0 \\ -\sin B \cos L & -\sin B \sin L & \cos B \\ \cos B \cos L & \cos B \sin L & \sin B \end{bmatrix} \quad (27)$$

where B is latitude and L is longitude.

2) UPDATING EQUATIONS

In section A, we know that four different satellites are necessary to ensure the final solution accuracy. Thus, there are two conditions: firstly, when the GNSS receiver receives new information and the number of different satellites is smaller than four, the first position has not been performed. At this time, the following equations are added in the formula (16) (28), as shown at the bottom of the page.

And formula (17) is updating to:

$$\begin{cases} x_1 = x_{k+1} - dx_{k+1,1}, y_1 = y_{k+1} - dy_{k+1,1}, z_1 \\ \qquad = z_{k+1} - dz_{k+1,1} \\ x_2 = x_{k+1} - dx_{k+1,2}, y_2 = y_{k+1} - dy_{k+1,2}, z_2 \\ \qquad = z_k - dz_{k+1,2} \\ \cdots \\ x_k = x_{k+1} - dx_{k+1,k}, y_k = y_{k+1} - dy_{k+1,k}, z_k \\ \qquad = z_{k+1} - dz_{k+1,k} \\ x_{k+1} = x_{k+1}, y_{k+1} = y_{k+1}, z_{k+1} = z_{k+1} \end{cases}$$
(29)

The second condition is the number of different satellites is bigger than 3. In this case, in addition to adding the equations (28), it is also important to determine whether the GNSS measurement is redundant. And we need to eliminate the redundant measurement and update formulas (16) and (17). The number series of the satellites at time k-th is

$$J_1 = \begin{bmatrix} \dfrac{-(x_{1,s1} - x_0)}{r_{1,s1}} & \dfrac{-(y_{1,s1} - y_0)}{r_{1,s1}} & \dfrac{-(z_{1,s1} - z_0)}{r_{1,s1}} \\ \vdots & \vdots & \vdots \\ \dfrac{-(x_{1,sn1} - x_0)}{r_{1,sn1}} & \dfrac{-(y_{1,sn1} - y_0)}{r_{1,sn1}} & \dfrac{-(z_{1,sn1} - z_0)}{r_{1,sn1}} \\ \cdots & \cdots & \cdots \\ \dfrac{-(x_{k,s1} - x_0 - dx_{k-1})}{r_{k,s1}} & \dfrac{-(y_{k,s1} - y_0 - dy_{k-1})}{r_{k,s1}} & \dfrac{-(z_{k,s1} - z_0 - dz_{k-1})}{r_{k,s1}} \\ \vdots & \vdots & \vdots \\ \dfrac{-(x_{k,snk} - x_0 - dx_{k-1})}{r_{k,snk}} & \dfrac{-(y_{k,snk} - y_0 - dy_{k-1})}{r_{k,snk}} & \dfrac{-(z_{k,snk} - z_0 - dz_{k-1})}{r_{k,snk}} \end{bmatrix}_{n \times 3}$$
(22)

$$\begin{cases} \sqrt{(x_{k+1,s1} - x_{k+1})^2 + (y_{k+1,s1} - y_{k+1})^2 + (z_{k+1,s1} - z_{k+1})^2} + t_{uk+1} = \rho_{k+1}, s1 \\ \vdots \\ \sqrt{(x_{k+1,snk+1} - x_{k+1})^2 + (y_{k+1,snk+1} - y_{k+1})^2 + (z_{k+1,snk+1} - z_{k+1})^2} + t_{uk+1} = \rho_{k+1,snk+1} \end{cases}$$
(28)

Algorithm 1 Calculating Position

Input: GNSS pseudo-range, satellite position, PDR data
Output: position
1: if first calculation is not done then
2:   if the number of different satellites is bigger than 3 then
3:     time align for PDR use the equation (24).
4:     updating equations.
5:     Compute position according to equations (21).
6:   end if
7: else
8:   time align for PDR use the equation (24).
9:   updating equations.
10:   Compute position according to equations (21).
11:   if GNSS measurement is redundant
12:     eliminate the redundant measurement.
13:     updating equations.
14:   end if
15: end if
16: output the position.

$U_k(SV_{k,1}, \ldots, SV_{k,nk})$. We use U_k and n_k to remove redundant data. The determining method is as follows:

$$flag_{sat} = \begin{cases} 1, & if\ (U_{k+1} = U_i \& n_{k+1} = n_i, k+1 > i) \\ 0, & otherwise \end{cases} \quad (30)$$

If $flag_{sat} = 1$, these equations at time i-th are redundant and they will be removed from formula (16). And the time (i + 1)-th becomes new i-th, then formula (17) updates to:

$$\begin{cases} x_1 = x'_k - dx'_{k,1}, y_1 = y'_k - dy'_{k,1}, z_1 = z'_k - dz'_{k,1} \\ \quad \vdots \\ x_{i-1} = x'_k - dx'_{k,i-1}, y_{i-1} = y'_k - dy'_{k,i-1}, z_{i-1} \\ \quad = z'_k - dz'_{k,i-1} \\ x'_i = x'_k - dx'_{k,i-1}, y'_i = y'_k - dy'_{k,i-1}, z'_i \\ \quad = z'_k - dz'_{k,i-1} \\ \quad \vdots \\ x'_{k-1} = x'_k - dx'_{k,k-1}, y'_{k-1} = y'_k - dy'_{k,k-1}, z'_{k-1} \\ \quad = z'_k - dz'_{k,k-1} \\ x'_k = x'_k, y'_k = y'_k, z'_k = z'_k \end{cases} \quad (31)$$

where $x'_k = x_{k+1}$ and $dx'_{k,1} = dx_{k+1,1}$. So the number of equations is reduced by $n_i + 3$.

The calculation position flow is shown as:

D. INTEGRATING PDR/GNSS

Although PDR has high precision within short periods, it is easily affected by accumulative errors. To achieve highly accurate positioning performance, it is essential to correct PDR in real-time. And even if the error of CalPos is bounded, it has large jumps. This paper designs a Kalman filter model to reduce systematic errors and correct PDR in real-time and smooth CalPos' error.

In this section, we integrate the output of PDR, CalPos and GNSS observations to obtain a fusion position using EKF. Here we use the position (x, y, z), velocity (v_x, v_y, v_z) and clock error of the GNSS receiver t_u:

$$X = [x, y, z, v_x, v_y, v_z, t_u] \quad (32)$$

The relationship of State variables is

$$\begin{cases} x(k+1) = x(k) + v_x(k+1)T + w_x(k+1) \\ y(k+1) = y(k) + v_y(k+1)T + w_y(k+1) \\ z(k+1) = z(k) + v_z(k+1)T + w_z(k+1) \\ v_x(k+1) = v_x(k) + w_{vx}(k+1) \\ v_y(k+1) = v_y(k) + w_{vy}(k+1) \\ v_z(k+1) = v_z(k) + w_{vz}(k+1) \\ t_u(k+1) = t_u(k) + w_{tu}(k+1) \end{cases} \quad (33)$$

where T is sample time. So state equation is established as:

$$X(k+1) = FX(k) + W(k+1) \quad (34)$$

where W is System error matrix, F is the transition matrix, which are shown in the Appendix A. We use the position (x, y, z), the velocity in NCS (v_e, v_n, v_u) and the pseudo-range $(\rho_1, \cdots, \rho_{ni})$ measured at time i-th to establish the observation vector:

$$Z = [x, y, z, v_e, v_n, v_u, \rho_1, \cdots, \rho_{ni}] \quad (35)$$

From section A, we know that the velocity in NCS is obtained as:

$$\begin{cases} v_e = SL_k * \sin(heading_k) \\ v_n = SL_k * \cos(heading_k) \\ v_u = \Delta h_k \end{cases} \quad (36)$$

The velocity transform from GCS to NCS as:

$$\begin{bmatrix} v_e \\ v_n \\ v_u \end{bmatrix} = (C_n^g)^T \begin{bmatrix} v_x \\ v_y \\ v_z \end{bmatrix} \quad (37)$$

The measurement equation is:

$$\begin{cases} x(k+1) = x(k) + v_x(k)*T + f_x(k+1) \\ y(k+1) = y(k) + v_y(k)*T + f_y(k+1) \\ z(k+1) = z(k) + v_z(k)*T + f_z(k+1) \\ v_e(k+1) = -\sin L \cdot v_x(k+1) + \cos L \cdot v_y(k+1) + f_e(k+1) \\ v_e(k+1) = -\sin B \cos L \cdot v_x(k+1) - \sin B \sin L \\ \quad \cdot v_y(k+1) \\ +\cos B \cdot v_z(k+1) + f_n(k+1) \\ v_u(k+1) = \cos B \cos L \cdot v_x(k+1) \\ \quad + \cos B \sin L \cdot v_y(k+1) \\ +\sin B \cdot v_z(k+1) + f_u(k+1) \\ \rho_1 = \sqrt{(x_s^1 - x)^2 + (y_s^1 - y)^2 + (z_s^1 - z)^2} + t_u \\ \quad \vdots \\ \rho_{ni} = \sqrt{(x_s^{ni} - x)^2 + (y_s^{ni} - y)^2 + (z_s^{ni} - z)^2} + t_u \end{cases}$$
$$(38)$$

GNSS Available:		
RTK:	Horizontal:0.02m	Vertical: 0.05m
Post-processing:	Horizontal:0.01m	Vertical: 0.02m
Single Point:	Horizontal:1.2m	Vertical: 0.6m
GNSS Outages in 60s:		
RTK:	Horizontal:0.72m	Vertical:0.55m
Post-processing:	Horizontal:0.04m	Vertical:0.03m
Inertial Sensors:	Gyroscope:	Accelerometer:
Measurement range	$\pm495º$	$\pm10g$
Bias(1σ)	<0.05º/hr	<100ug
scale factor(1σ)	<100ppm	<100ppm

It is simplified as:

$$Z\,(k+1) = HX\,(k+1) + Y\,(k+1) + V\,(k+1) \quad (39)$$

where V is the observation error matrix, Y is the input, and the H matrix is the coefficient matrix, which is shown in Appendix A.

III. PERFORMANCE EVALUATION

A. EXPERIMENTAL ENVIRONMENT

To evaluate the proposed scheme's performance in real environments, we use Huawei Mate 20 to do experiments. During the experiment, the smartphone is held in hand, and its x-axis is in the forward direction. We use the GNSS Inertial Systems product produced by Novatel to calculate the post-processing reference trajectory, consisting of the GNSS receiver (Novatel ProPak7 receiver), Novatel GPS-704 antenna, and IMU-ISA-100. In the experiment, ProPak7 is a high-precision receiver that can receive five satellite systems (GPS, GLONASS, BeiDou, Galileo, and QZSS). The Mate 20 is used to collect raw data of acceleration, rate of turn, magnetic field, and barometer at 20Hz and pseudo-range of GNSS at 1Hz. The main technical specifications of GNSS Inertial Systems are listed in Table 1.

We complete the experiment at the New Technology Facility Campus of the Chinese Academy of Sciences, a typical urban canyon with dense foliage and tall buildings. The testing route is shown in Fig. 5. It starts from the outdoor, as shown in the figure. The pedestrian passes through a section of buildings and trees dense environment, as shown in mark one and mark two. Then it enters the underground garage where there is no signal of satellite as shown in mark three. At last, it comes out to return to the origin point. It total takes about 10 minutes.

The output of the Novatel ProPak7 receiver and smartphone is shown in Fig. 6. The green points represent GNSS, which results from the original satellite data collected by mobile phone without satellite selection. The blue points represent the Single Point (SP) of ProPak7. The red points are the post-processing of GNSS Inertial Systems, which will be the baseline. The statistics of root mean square (RMS) errors and mean error are shown in Table 2. Availability means the percentage of solutions in a fixed period. For instance, if a method outputs 100 epochs in a 100 second period, the method's availability is 100%.
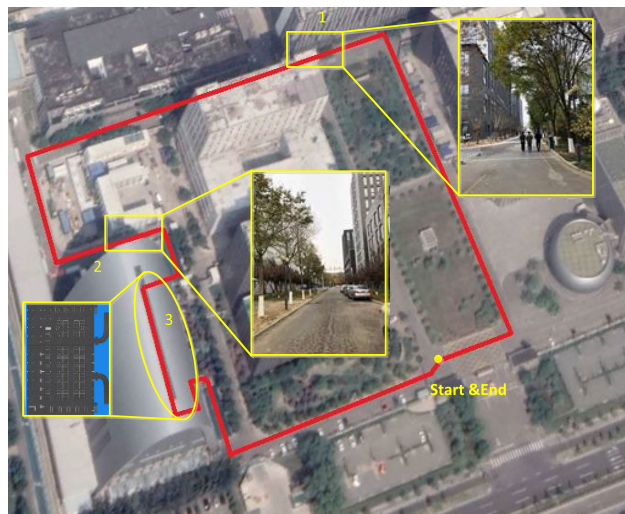

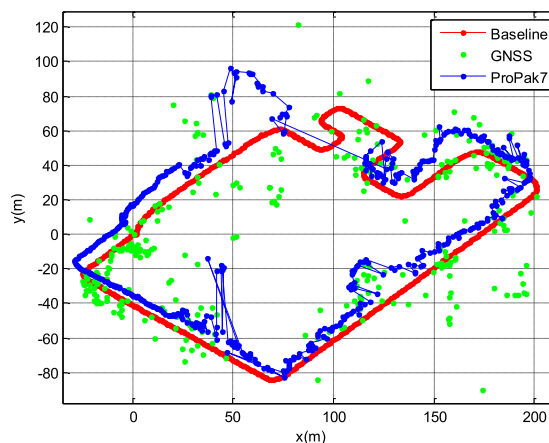**FIGURE 5.** Demonstration of the target deep urban canyon with dense foliage.

FIGURE 6. Positioning result of GNSS of smartphone and ProPak7.

TABLE 2. Positioning Performance of Smartphone and Propak7.

Equipment	Performance		
	RMS	Mean	Avail.
GNSS (Smartphone)	51.7m	57.4m	54.83%
SP (ProPak7)	18.5m	15.6m	79.13%

As shown in Table 2, the positioning error's standard deviation of ProPak7 is about 18.5m, which means GNSS cannot achieve satisfactory performance using the data attenuated by dense foliage because of the degrading of signal transmission, notorious multipath effects, and NLOS reception. As it takes more than 2 min in the underground garage, the availability of ProPak7 is 79.13%. The performance of the smartphone is far worse than ProPak7. The standard deviation of positioning error is 51.7m, and the availability is 54.83%.

B. EXPERIMENAL RESULTS

1) RESULTS OF CALCULATING POSITION

This paper proposes an algorithm to calculate the position based on satellite observation measurement and PDR at different times. And it is significant to select effective satellites
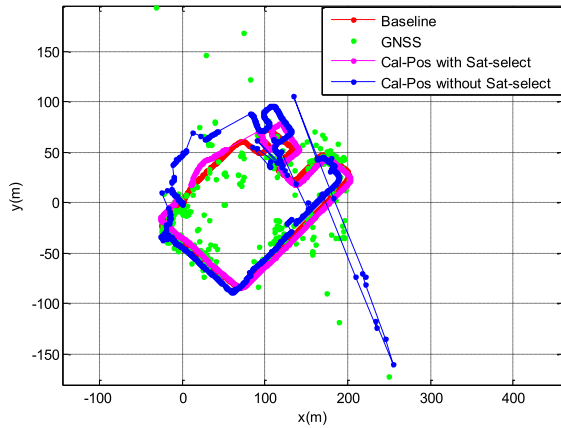
FIGURE 7. Result of CalPos with and without satellite selecting. The pink points are the result of CalPos with satellite selecting, and the blue points are the result without ones.
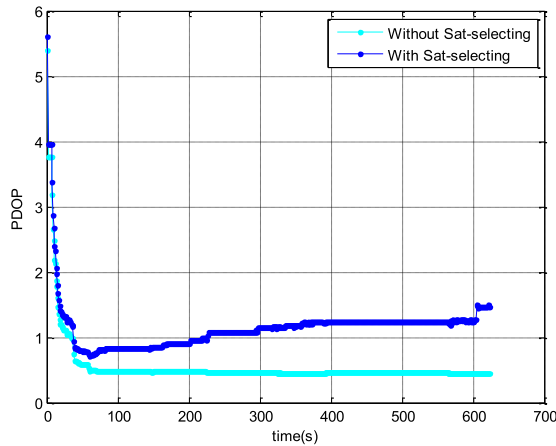

FIGURE 8. The PDOP series of CalPos with and without satellite selecting.

TABLE 3. Positioning Performance of CalPos.

Approach	Performance		
	RMS	Mean	Avail
with satellite selecting	15.8m	12.2m	100%
without satellite selecting	44.8m	27.3m	100%

before CalPos. The results with and without satellite selection are shown in Fig. 7. Obviously, the positioning performance of CalPos proposed in this paper is better than GNSS, and the result with satellite selecting is better than without one. In addition, as shown in Fig. 8, even though the equations are established without satellite selection, and the PDOP of CalPos is significantly better than that with ones, which is about 0.5, the performance of that is worse. The main reason is that inferior satellites are added into the equations, which means signal blockage and notorious multipath errors are added into the result of CalPos. As shown in Table 3, the standard deviation of satellite selecting is 15.8m, which is better than the SP of ProPak7. In addition, comparing Table 2, the availability increases from 54.83% to 100%.

To further analyze the influence of the satellites' number on the positioning performance, we count the errors under

TABLE 4. Positioning performance under different number of satellites.

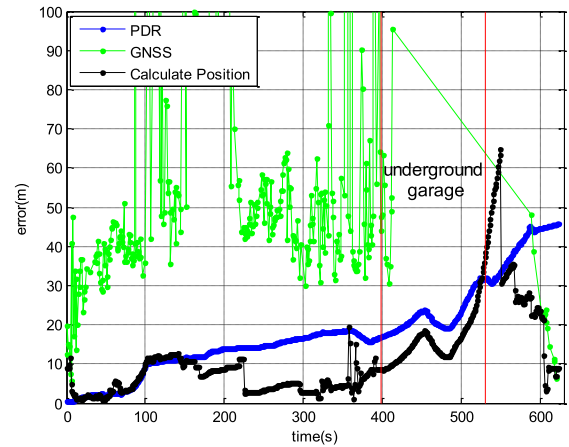| Number of satellites	Error	
	RMS	Mean
0 satllite	19.1m	12.6m
1-3 satllites	12.7m	9.4m
≥4 satllites	1.5m	1.4m

FIGURE 9. The Position error series of CalPos with satellite selecting.

the different number of satellites, as shown in Table 4. From the table, we know that the more effective satellites are inputted into the equations of CalPos, the better the position performance is. Especially when the number of satellites is more than 3, the positioning accuracy is greatly improved, which is about 1.5m. On the contrary, as shown in Table 3, if the inferior satellite is used to calculating position, the more satellites are used, the bigger the error is. It shows that the current user's position calculating with historical observation data is related to the new observation information, including the number of satellites and the quality of the signal.

According to Fig. 9, the error variation trend of Calpos is related to the PDR error, especially the indoor, where there is no satellite signal. As shown in Fig. 8 and Fig. 9, when there is not much historical data available, the position error varies according to the PDR error, and the influence of PDOP is small. On the contrary, when the more historical observation is used to solve position, the more the error is related to PDOP, but not to PDR. When the user is indoors, there is no satellite signal, and the position solution only uses the historical satellite information without new GNSS observation. Since only the PDR error is introduced into the solution, the error trend of CalPos is almost the same as PDR's. In addition, owing to losing satellite signal for a long time, the error will be divergent for a period of time when the user leaves the indoor environment, as shown in Fig.9. With the increase of satellite observation data, the error will converge slowly.

As we use satellite observation at different times to calculate position, the number of epochs used in CalPos is a significant interfering factor of error, as shown in Fig. 10. When the epoch number is less than 8, the position error is more than 100m, not shown in the figure. When the number
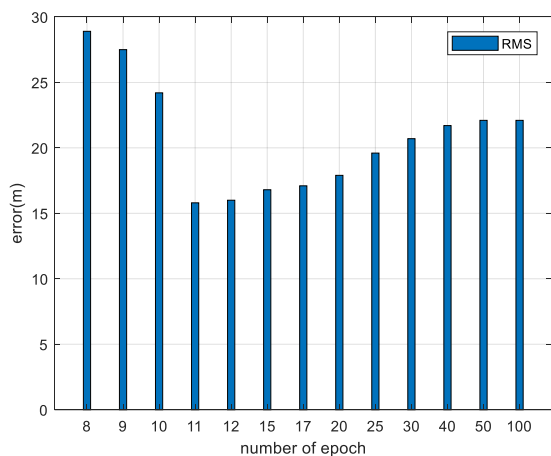
FIGURE 10. The Position error series of CalPos with satellite selecting.

is smaller than 11, the more epochs are used, the better the performance is. The performance becomes worse when the number is bigger than 20. If the number of epochs is bigger than 40, the position error is not affected by it. As shown in Fig. 10, the position error is affected by the number of epochs a little between 11 and 20. Considering the accuracy, efficiency and complexity of the calculation, the maximum number of epochs involved in the equations is 11.

2) RESULTS OF INTEGRATING PDR/GNSS

This paper proposes a comprehensive strategy for fusing CalPos, GNSS observations and PDR, which use satellite observations at different times. As shown in Fig.11 (a), the error variation trend is related to the CalPos. Through integrating PDR/GNSS, the most jumps that exist in the CalPos positions are removed. And when PDR and CalPos are divergent, the proposed method has slower divergence and faster convergence. When there is no GNSS signal, the positioning error can also be corrected to reduce with filter. After re-adding satellite information, the fusion result will be gradually corrected according to the increase of satellite observation information.

The Cumulative distribution function (CDF) graph is shown in Fig. 11(b). Our proposed fusion scheme obtains 80% positioning error below 10m, whereas the PDR's positioning error is no more than 20%, and the CalPos's is about 60%. According to Table 5, the standard deviation of Integrated PDR/GNSS is 9.6m, and the average error is 7.6m. Comprising with PDR and CalPos, the position error is increased by 48% and 39%, respectively. By comparing and analyzing the overall positioning performance, we can see that the method proposed in this paper can provide a continuous and stable localization scheme.

C. DISCUSSION

To better present the proposed system's effectiveness and performance, we compare with five methods in reference. For a fair comparison, they use the same set of data for calculation and statistical error, as shown in Fig. 12 and Table 6. As can be seen, owing to using GNSS observation at different times,
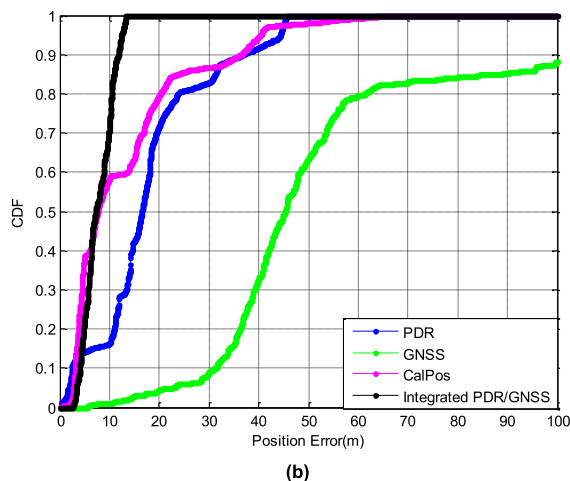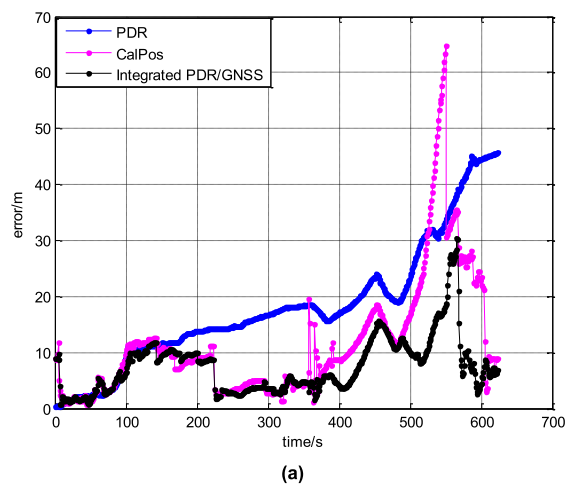

FIGURE 11. (a) positioning error,(b) CDF of the positioning error.

the proposed algorithm has the best performance comprising the reference methods. On the contrary, the method proposed in reference [6] has the worst positioning accuracy because it only uses GNSS to correct the motion direction. As PDR/GPS [15], MIMU/GPS [7] and GloPos[5] algorithm use the fusing method to reduce the noise error, which can achieve better positioning accuracy than PDR/GNSS [6]. Triggered INS/GNSS[11] proposed an event-triggered multi-rate size-varying Kalman filter model, which can remove systematic errors due to the wrong calibration of the sensors or environmental noises and solve the integrated problem when sampling rates of each source is different. So, it can achieve much better performance than the other four methods as 23.4m. When the pedestrian walks in an open area with adequate GNSS signals, these methods can achieve high accuracy, which has been tested in the reference. However, when it is in a harsh environment, such as dense forests, and densely built urban areas, where the GNSS position error is vast due to signal blockage and multipath, their error will also be vast. As the algorithm in this paper is specially designed for this situation, it has better positioning performance.

Some other fusion methods have been proposed and tested to deal with the problem of signal transmission degradation

TABLE 5. Error analysis of different positioning methods.

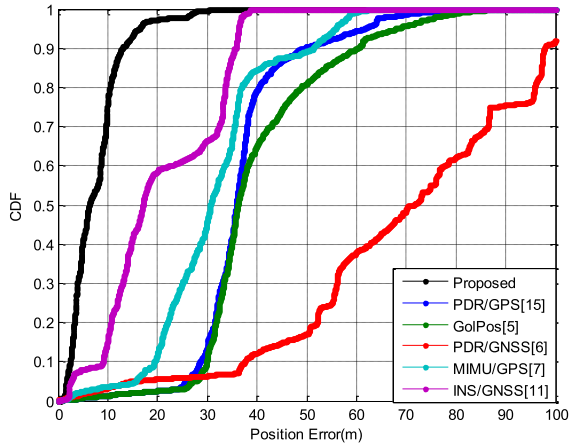| Mathod	Performance		
	RMS	mean	Avail
PDR	18.6m	18.1m	100%
Integrated PDR/GNSS	9.6m	7.6m	100%

FIGURE 12. The Position error series of CalPos with satellite selecting.

and multipath effects in deep urban canyons. In order to analyze the effectiveness and performance of the proposed system, we compare them in Table 7. As these methods basically introduce external assistance, we do not reproduce them. As shown in the table, PDR + 3D Map + GNSS [3] has the best accuracy, using the 3D Map to assist GNSS. It can achieve high accuracy because the error of the 3D Map will not be affected by the environment. According to the table, although the proposed algorithm only uses GNSS and PDR,

TABLE 6. Comparison of location errors for PDR/GNSS.

Method	Error(RMS)
Smartphone-based PDR/GPS[15]	38.5m
GloPos[5]	42.3m
PDR/GNSS [6]	74.9m
MIMU/GPS[7]	33.5m
Triggered INS/GNSS[11]	23.4m
Proposed	9.6m

TABLE 7. Comparison of location errors for different methods.

Method	RMS
Proposed	9.6m
PDR/PDD[14]	10.7m
GNSS+PDR+beacon[13]	10m&15m
PDR + 3D map+GNSS [3]	2.5m

it can achieve the same performance with GNSS + PDR + beacon [13] and PDR/PDD [14], which use extern beacon and base station to assist PDR/GNSS to achieve high accuracy.

IV. CONCLUSION

Due to dense foliage and tall buildings' attenuation in deep urban canyons, only a few satellites are reliable. In this paper, we propose a comprehensive strategy for fusing GNSS observations and PDR, which use satellite observations at different times to solve the localization problem. Firstly, we propose a pedestrian localization algorithm based on PDR and GNSS observations at different times, using the smartphone's internal sensors. It can improve accuracy and continuity and solve missing data, such as without satellite coverage. Secondly, an

$$W = \left[w_x, w_y, w_z, w_{vx}, w_{vy}, w_{vz}, w_{tu} \right]$$

$$F = \begin{bmatrix} 1 & 0 & 0 & T & 0 & 0 & 0 \\ 0 & 1 & 0 & 0 & T & 0 & 0 \\ 0 & 0 & 1 & 0 & 0 & T & 0 \\ 0 & 0 & 0 & 1 & 0 & 0 & 0 \\ 0 & 0 & 0 & 0 & 1 & 0 & 0 \\ 0 & 0 & 0 & 0 & 0 & 1 & 0 \\ 0 & 0 & 0 & 0 & 0 & 0 & 1 \end{bmatrix} \tag{40}$$

$$H = \begin{bmatrix} 1 & 0 & 0 & T & 0 & 0 & 0 \\ 0 & 1 & 0 & 0 & T & 0 & 0 \\ 0 & 0 & 1 & 0 & 0 & T & 0 \\ 0 & 0 & 0 & -\sin L & \cos L & 0 & 0 \\ 0 & 0 & 0 & -\sin B \cos L & -\sin B \sin L & \cos B & 0 \\ 0 & 0 & 0 & \cos B \cos L & \cos B \sin L & \sin B & 0 \\ \frac{\partial f_1}{\partial x}\big|_{p0} & \frac{\partial f_1}{\partial y}\big|_{p0} & \frac{\partial f_1}{\partial z}\big|_{p0} & 0 & 0 & 0 & 1 \\ \vdots & \vdots & \vdots & \vdots & \vdots & \vdots & 1 \\ \frac{\partial f_{ni}}{\partial x}\big|_{p0} & \frac{\partial f_{ni}}{\partial y}\big|_{p0} & \frac{\partial f_{ni}}{\partial z}\big|_{p0} & 0 & 0 & 0 & 1 \end{bmatrix} \tag{41}$$

$$Y(k+1) = \begin{bmatrix} 0_{3\times 1} \\ f_0 - J_1 \left[x_0, y_0, z_0 \right]^T - t_{u0} \end{bmatrix}, f_0 = \left[r_{k+1,1}^0, \ldots, r_{k+1,ni}^0 \right]^T \tag{42}$$

$$V = \left[f_e, f_n, f_u, f_{\rho 1}, \ldots, f_{\rho n} \right]^T \tag{43}$$

equation update method for different situations is presented because the algorithm presented in this paper is different from traditional ones. In addition, a Kalman filter model is designed to reduce systematic errors and correct cumulative error of PDR in real-time. Then we perform tests in a typical urban canyon to verify its positioning capability. By comparing and analyzing the overall positioning performance, the method proposed in this paper can provide the optimal navigation scheme.

This paper proves a comprehensive strategy for fusing historical GNSS observations and PDR is useful even if the number of reliable satellites is few. However, when the GNSS signals become very difficult to be received, the error of fusion will be growing with time. When the pedestrian comes out from the indoor and satellite information is re-received, the fusion result will be gradually corrected according to the increase of satellite observation information. Our future work is to find move efficient method to solve those problems.

APPENDIX
See Equations (40)–(43).

REFERENCES
[1] M. G. Petovello, and P. D. Groves, "GNSS solutions: Multipath vs. NLOS signals. How does non-line-of-sight reception differ from multipath interference," in *Inside GNSS*. Dec. 2013, pp. 40–42. [Online]. Available: https://insidegnss.com/multipath-vs-nlos-signals/
[2] W. Kang and Y. Han, "SmartPDR: Smartphone-based pedestrian dead reckoning for indoor localization," *IEEE Sensors J.*, vol. 15, no. 5, pp. 2906–2916, May 2015.
[3] L.-T. Hsu, Y. Gu, and S. Kamijo, "Sensor integration of 3D map aided GNSS and smartphone PDR in urban canyon with dense foliage," in *Proc. IEEE/ION PLANS*, Savannah, GA, USA, Apr. 2016, pp. 85–90.
[4] B. Li, C. Xu, X. Li, H. Zhang, and W. Wang, "BeiDou navigation satellite system in challenge environment using an atomic clock and barometric altimeter," *J. Electron. Inf. Technol.*, vol. 40, no. 9, pp. 2212–2218, 2018.
[5] C. Wu, Z. Yang, Y. Xu, Y. Zhao, and Y. Liu, "Human mobility enhances global positioning accuracy for mobile phone localization," *IEEE Trans. Parallel Distrib. Syst.*, vol. 26, no. 1, pp. 131–141, Jan. 2015.
[6] H. Lan, C. Yu, and E. Naser, "An integrated PDR/GNSS pedestrian navigation system," in *Proc. CSNC*, Xi'an, China, 2015, pp. 677–690.
[7] W. Sun, D. Liu, and Y. Liu, "Fusion method of Android terminal based on PDR/GPS," *Sci. Surv. Mapping*, vol. 43, no. 12, pp. 118–122, 2018.
[8] A. Rehman, H. Shahid, M. A. Afzal, and H. M. A. Bhatti, "Accurate and direct GNSS/PDR integration using extended Kalman filter for pedestrian smartphone navigation," *Gyroscopy Navigat.*, vol. 11, no. 2, pp. 124–137, Apr. 2020.
[9] G.-H. Tian, Q.-B. Zhang, and N.-N. Ding, "Research on integrated positioning of PDR and GPS based WT-UKF," *Control Decis.*, vol. 30, no. 1, pp. 86–90, 2015.
[10] H. Niu and B. Lian, "An integrated positioning method for GPS+PDR based on improved UKF filtering," *Bull. Surv. Mapping*, vol. 7, pp. 5–9, Jul. 2017.
[11] M. Basso, M. Galanti, G. Innocenti, and D. Miceli, "Triggered INS/GNSS data fusion algorithms for enhanced pedestrian navigation system," *IEEE Sensors J.*, vol. 20, no. 13, pp. 7447–7459, Jul. 2020.
[12] F. Zhu, X. Tao, W. Liu, X. Shi, F. Wang, and X. Zhang, "Walker: Continuous and precise navigation by fusing GNSS and MEMS in smartphone chipsets for pedestrians," *Remote Sens.*, vol. 11, no. 2, pp. 1–16, Jan. 2019.
[13] J. Ye, Y. Li, H. Luo, J. Wang, W. Chen, and Q. Zhang, "Hybrid urban canyon pedestrian navigation scheme combined PDR, GNSS and beacon based on smartphone," *Remote Sens.*, vol. 11, no. 18, pp. 1–26, 2019.
[14] Z. Wu, P. Liu, Q. Liu, Y. Wang, J. Qian, and H. Zhu, "Fusion algorithm of pseudo range double difference and PDR based on original observation of GNSS," in *Proc. CSNC*, Beijing, China, 2019, pp. 1–7.

[15] X. Li, D. Wei, Q. Lai, Y. Xu, and H. Yuan, "Smartphone-based integrated PDR/GPS/bluetooth pedestrian location," *Adv. Space Res.*, vol. 59, no. 3, pp. 877–887, 2017.
[16] *U.S. Standard Atmosphere*, Nat. Ocean. Atmos. Admin., U.S. Government Printing Office, Washington, DC, USA, 1976.
[17] K. Liu, Y. Wang, and J. Wang, "Differential barometric altimetry assists floor identification in WLAN location fingerprinting study," in *Principle and Application Progress in Location-Based Services*. Berlin, Germany: Springer, Jul. 2014, pp. 21–29.
[18] L. Zheng, W. Zhou, W. Tang, X. Zhang, A. Peng, and H. Zheng, "A 3D indoor positioning system based on low-cost MEMS sensors," *Simul. Model. Pract. Theory*, vol. 19, pp. 45–56, Feb. 2016.
[19] Y. Wang, "Study on fast satellite selection algorithm for GNSS navigation system," *Electron. Des. Eng.*, vol. 26, no. 3, pp. 65–69, 2018.
[20] J. Liu, X. Zhang, and Y. Xu, "Satellite selection algorithm for combined GPS and GLONASS single point positioning," *J. Geomatics*, vol. 37, no. 2, pp. 4–6, 2012.
[21] G. Xie, *Principles of GPS and Receiver Design*, vol. 101. Beijing, China: Publishing House of Electronics Industry, 2009, pp. 70–71.
[22] B. Yu, Y. Chen, and X. Guo, *Inertial Technology*. Beijing, China: Beihang Univ. Press, 1994, pp. 214–215.
[23] A. Rehman, Q. Liu, Z. Wu, H. Zhu, J. Qian, Y. Wang, and P. Liu, "PDR/GNSS fusion algorithm based on joint heading estimation," in *Proc. CSNC*, Beijing, China, 2019, pp. 326–339.
[24] M. Zhang, Y. Wen, J. Chen, X. Yang, R. Gao, and H. Zhao, "Pedestrian dead-reckoning indoor localization based on OS-ELM," *IEEE Access*, vol. 6, pp. 6116–6129, 2018.
[25] J. Seitz, T. Vaupel, J. Jahn, S. Meyer, J. G. Boronat, and J. Thielecke, "A hidden Markov model for urban navigation based on fingerprinting and pedestrian dead reckoning," in *Proc. FUSION*, Edinburgh, U.K., Jul. 2010, pp. 1–8.
[26] S. Zhang, "Research on GNSS measurement and GNSS/PDR fusion algorithm for Android smart phone," M.S. thesis, Dept. Geodesy Surv. Eng., China Univ. Mining Technol., Beijing, China, 2020.
[27] P. Peltola, J. Xiao, T. Moore, A. R. Jiménez, and F. Seco, "GNSS trajectory anomaly detection using similarity comparison methods for pedestrian navigation," *Sensors*, vol. 18, no. 9, pp. 1–26, 2018.
[28] R. Zhu, Y. Wang, H. Cao, B. Yu, X. Gan, L. Huang, H. Zhang, S. Li, H. Jia, and J. Chen, "RTK/pseudolite/LAHDE/IMU-PDR integrated pedestrian navigation system for urban and indoor environments," *Sensors*, vol. 20, no. 6, pp. 1–22, 2020.

XIANGHONG LI received the B.S. and M.S. degrees from the School of Automation Science and Electrical Engineering, Beihang University, in 2014. She is currently pursuing the Ph.D. degree in signal and information processing with the Chinese Academy of Sciences, Beijing, China. Since 2014, she has been an Engineer with the Academy of Opto-Electronics, Chinese Academy of Sciences, Beijing. Her research interests include position indoor, pedestrian dead reckoning (PDR), integrated navigation, and information fusion.
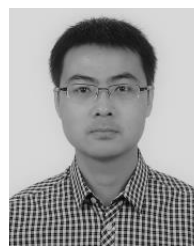
DONGYAN WEI received the B.S. degree in communication engineering from the University of Electronic Science and Technology of China (UESTC), in 2006, and the Ph.D. degree in signal and information processing from the Beijing University of Post and Telecommunication (BUPT), in 2011. He is currently a Research Fellow with the Aerospace Information Research (AIR) Institute, Chinese Academy of Sciences (CAS). He is the author of one book, more than 30 articles, and more than 20 inventions. His research interests include indoor position, multi-sensor fusion, and positing in wireless networks. He is a TPC member of IPIN 2019 and the Deputy Chair of IPIN 2022.

WENCHAO ZHANG received the B.S. degree in surveying engineering from the China University of Mining and Technology (CUMT), in 2013, the M.S. degree in surveying engineering from Information Engineering University, in 2016, and the Ph.D. degree in signal and information processing form the University of Chinese Academy of Sciences (UCAS), in 2020. He is currently with the Aerospace Information Research (AIR) Institute, Chinese Academy of Sciences (CAS). His research interests include multi-information fusion method, integrated navigation algorithm, pedestrian autonomous positioning algorithm based on MEMS sensors, and pedestrian indoor positioning method based on inertial sensors.

YING XU received the Ph.D. degree in signal processing from the Beijing Institute of Technology, China, in 2009. She is currently a Research Professor and a Doctoral Supervisor of the Navigation System Department, Aerospace Information Research Institute, Chinese Academy of Sciences. Her research interests include satellite navigation technology and its augmentation technology, and multi-source fusion localization theory and methods.

HONG YUAN received the Ph.D. degree from the Shanxi Astronomical Observatory, Chinese Academy of Sciences, in 1995. From 1995 to 2004, he worked at the Wuhan Institute of Physics and Mathematics, Chinese Academy of Sciences. In 2004, he was transferred to the Academy of Opto-Electronics (AoE), Chinese Academy of Sciences. For many years, he has been engaged in research on ionospheric radio wave propagation, GPS, Beidou satellite navigation system construction, manned space applications, ionospheric physics, and ionospheric detection. He is currently a Research Fellow with the Aerospace Information Research (AIR) Institute, Chinese Academy of Sciences. He is currently engaged in software and hardware design and algorithm research related to satellite navigation, multi-source fusion navigation, and ionospheric detection. He has hosted or participated in 13 national and provincial level projects, eight provincial and ministerial science and technology awards, holds more than 30 invention patents, and has published more than 60 articles.

● ● ●